Renormalization-group acceleration of self-consistent field solutions: Two-dimensional Hubbard model

Chien-Hua Pao and N. E. Bickers
Department of Physics, University of Southern California, Los Angeles, California 90089
(Received 29 July 1993)

Momentum- and frequency-dependent self-consistent field theories provide a potentially powerful tool for analyzing condensed-matter models for interacting electrons. Such theories generally require the solution of multidimensional integral equations. Solutions are limited by demands on computational time and storage, which increase rapidly for calculation of low-temperature properties. A renormalization-group technique which allows the sequential elimination of regions of high frequency and momentum is presented in detail, and is then applied to the solution of the fluctuation exchange approximation for the two-dimensional Hubbard model. Effective meshes with as many as 10^4 frequencies and 512^2 **k** points can be analyzed on a vector supercomputer using this approach. As a sample application, it is demonstrated that the fluctuation exchange approximation exhibits non-Fermi liquid behavior near half filling for sufficiently large interaction strengths.

I. INTRODUCTION

The thermodynamic and transport properties of a number of experimentally interesting materials, including the heavy electron metals and cuprate superconductors, are believed to be strongly influenced by the presence of short-range electron-electron correlations.[1] The simplest model which incorporates the effect of local Coulomb repulsion on states in an electronic band is the Hubbard model.[2] Numerous theoretical techniques have been used to investigate the low-temperature properties of this model and its generalizations. Direct numerical approaches include exact diagonalization of the Hamiltonian matrix and quantum simulation. The principal restriction on these methods is the presence of finite-size effects for small systems.

Self-consistent field (SCF) theories provide a partially analytical alternative to the direct approaches.[3–8] SCF methods are not restricted by size effects, but are limited by the necessity for approximations. By comparing results for correlation functions with simulation studies,[5,7,8] it has been possible to demonstrate the semiquantitative (and in some cases, quantitative) validity of certain Hubbard-model SCF approximations in a wide parameter range. This opens the possibility of using SCF methods to study more detailed models which are not well suited to large-scale study by simulation techniques.

General SCF theories require the solution of multidimensional integral equations on a finite grid. Computational problems associated with rapid growth in the number of grid points at low temperatures constitute the principal limitation on future applications. In the present paper we address this problem by formulating a renormalization-group (RG) technique for the sequential solution of SCF equations on multiple frequency and momentum scales. This approach is not limited by details of the approximation or the model, but is here applied in detail to the so-called fluctuation exchange (FLEX) approximation for the two-dimensional (2D) Hubbard model.[3–6] The paper is organized as follows: In Sec. II we briefly review the rationale for SCF generalizations of Hartree-Fock theory and discuss the motivation for developing accelerated solution techniques. In Sec. III we describe our RG prescriptation in detail, addressing first the removal of high-frequency regions of parameter space and then the removal of high-momentum regions. In Sec. IV we present a comparison of results for one-particle correlation functions obtained with and without use of the RG technique. As an aside, we briefly discuss the appearance of non-Fermi liquid behavior in the one-electron self-energy for a range of parameters. Finally, we conclude with a brief summary in Sec. V.

II. MOTIVATION FOR ACCELERATING SCF SOLUTIONS

SCF theories have long played a central role in the approximate solution of models for interacting electrons in solids. Such theories vary considerably in complexity. In many cases a *qualitatively* correct description of properties may be obtained by examining the interaction of electrons with a time-averaged background (the so-called Hartree, or Hartree-Fock, approximation). In simple cases the electron-electron interaction is instantaneous and only weakly dependent on momentum transfer (as, for example, in simple theories of itinerant ferromagnetism). Hartree-Fock approximations may also be formulated for frequency-dependent effective interactions, such as that which arises from the exchange of phonons. Migdal's theory of phonon corrections to the electronic normal state[9] and Eliashberg's extension of this theory to the superconducting state[10] are examples of highly successful frequency-dependent Hartree-Fock approximations.

Hartree-Fock approximations are generally not *quantitatively* accurate. Exceptions rely on the existence of a small parameter, such as the ratio of the phonon Debye

energy and electronic Fermi energy in the Migdal-Eliashberg approach. The chain of reasoning which rules out the need for fluctuation corrections to the averaged background in these exceptional cases is sometimes known as Migdal's theorem.[9] Such a theorem can only be expected in systems with a strongly retarded effective interaction. Narrow-band systems, in which the Coulomb interaction between electrons must be treated from first principles (rather than replaced by a pseudopotential), automatically violate the requirements for Migdal's theorem, and so are expected to be poorly described by a Hartree-Fock approximation.

A number of extensions of the SCF approach for narrow-band systems have been proposed in recent years.[11] These approaches have proceeded from the following assumption: The violation of Migdal's theorem for the unrenormalized interactions (i.e., the "bare" Coulomb interactions between electrons) requires the introduction and self-consistent treatment of multielectron excitations. The simplest such excitations are just electron-hole and electron-electron pairs. The propagators for these pairs are infinite order in the Migdal expansion parameter, so the approach is from the outset essentially different from a low-order correction of the Hartree-Fock approximation by "vertex corrections."

The simplest extension of the Hartree-Fock approximation which remains within the family of conserving Baym-Kadanoff approximations[12] and incorporates interaction with electron-hole (and, optionally, electron-electron) pairs has been called the fluctuation exchange, or FLEX, approximation.[3] The FLEX approximation may be viewed in turn as the first step in the solution of a more general "parquet approximation" for one- and two-electron correlation functions.[5,7]

The principal difficulties with implementing these self-consistent generalizations of Hartree-Fock theory are computational, rather than conceptual. Since the interactions experienced by an individual electron are highly nonlocal in space and time, the self-consistency conditions take the form of integral equations in $d+1$ dimensions, with d the spatial dimensionality. So long as electron motion is restricted to a discrete set of orbitals on a periodic lattice, the spatial degrees of freedom may be conveniently Fourier-transformed, producing a bounded Brillouin zone. The number of electronic bands just corresponds to the number of orbitals per unit cell (one, for the simplest Hubbard models). If thermodynamic properties are of interest (or if one is willing to calculate dynamic properties by numerical analytic continuation), it is convenient to perform a Wick rotation on the time variables and then to Fourier-transform to imaginary (Matsubara) frequencies. At finite temperatures, the allowed frequencies of the temperature-averaged electronic correlation functions are *discrete* and take the values $\omega_n=(2n+1)\pi T$, with T the system temperature. Since the number of allowed frequencies is still infinite, temperature-independent imaginary-axis cutoffs must be established for numerical calculations.

At high temperatures a coarse momentum-space discretization is sufficient to obtain high numerical accuracy, and the number of Matsubara frequencies which fit within the cutoff range is small. In this case computational storage and time requirements may be minimal. However, as the temperature decreases, an increasingly fine momentum-space mesh is generally required to obtain accurate results, particularly in the region of the Fermi surface, where correlation functions vary rapidly. Furthermore, the number of required Matsubara frequencies within a fixed cutoff is inversely proportional to the system temperature. The requirements of decreasing temperature rapidly begin to tax the storage and speed capabilities of even the largest computers. Increased computational efficiency is clearly essential, particularly for the treatment of models with realistic orbital structures and Coulomb interactions.

In certain cases time requirements for SCF calculations may be reduced drastically from "brute-force" estimates by the use of fast Fourier transforms (FFT's).[6] Studies of the FLEX approximation for the two-dimensional Hubbard model have demonstrated the power of this approach, which leads to a reduction from $O(N^2)$ to $O(N \ln N)$ in scaling with the size of the variable domain N. The FFT's utility is limited, however, to approximations in which time requirements are dominated by the computation of convolution integrals. Baym-Kadanoff approximations for more complex models and general parquetlike approximations are dominated instead by the computation of matrix inverses, for which FFT methods are not applicable. Furthermore, the FFT approach leads to no reduction in storage requirements.

An appealing alternative approach to dealing with the proliferation of mesh points in general SCF theories is provided by renormalization-group concepts. The central idea, as in all numerical RG applications, is that the need for increasing magnification is not uniform throughout the space of interest (in this case, frequency and momentum space). Correlation functions evaluated at high frequencies or at momentum points distant from the Fermi surface eventually become temperature independent as the temperature is reduced. The temperature below which variations "freeze out" depends on the particular values of ω_n and $\mathbf{k}$ selected. Regions of frequency and momentum may therefore be sequentially removed from calculations. To study the low-temperature limit, it is only necessary to tabulate the values of correlation functions at their lowest "active" temperatures and then to carry forward temperature-independent contributions from the eliminated regions to functions in the remaining active regions. As regions of high frequency and momentum are eliminated, it becomes feasible to increase the magnification scale in those regions which remain without greatly increasing time or storage requirements.

In the sections which follow we describe explicitly a RG prescription for solving the two-dimensional Hubbard model at arbitrary filling within the FLEX approximation, and compare results for one-particle correlation functions obtained with and without the RG. The prescription is not specific to the Hubbard model or to the FLEX approximation, but could be used to accelerate the solution of any Baym-Kadanoff approximation for an electronic normal state.

III. RENORMALIZATION-GROUP APPROACH FOR THE FLEX APPROXIMATION

The Hamiltonian of the simplest 2D Hubbard model takes the form

$$\mathcal{H}=-t\sum_{\langle ij\rangle\sigma}(c_{i\sigma}^{\dagger}c_{j\sigma}+\text{H.c.})+U\sum_{i}n_{i\uparrow}n_{i\downarrow}-\mu\sum_{i\sigma}n_{i\sigma}\ , \tag{1}$$

where t is the nearest-neighbor hopping integral, U is an on-site Coulomb repulsion, and μ is the chemical potential. The one-electron Green's function may be written

$$G(\mathbf{k},i\omega_n)=[G_0^{-1}(\mathbf{k},i\omega_n)-\Sigma(\mathbf{k},i\omega_n)]^{-1}\ , \tag{2}$$

where

$$G_0(\mathbf{k},i\omega_n)=[i\omega_n-(\varepsilon_{\mathbf{k}}-\mu)]^{-1} \tag{3}$$

and $\Sigma(\mathbf{k},i\omega_n)$ is the self-energy. Note that ω_n is a fermion Matsubara frequency, i.e.,

$$\omega_n=(2n+1)\pi T\ , \tag{4}$$

with n an integer and T the system temperature.

In writing down the FLEX approximation[3] for the self-energy, it is convenient to introduce the notation

$$k\equiv(\mathbf{k},i\omega_n)\ ,\qquad \int_k\equiv\frac{1}{N}\sum_{\mathbf{k}}T\sum_{\omega_n}\ . \tag{5}$$

The FLEX self-energy[13] (see Fig. 1) is

$$\Sigma(k)=\int_{k'}V_{\text{eff}}(k-k')G(k')\ , \tag{6}$$

where

$$V_{\text{eff}}(q)=U^2\chi(q)+\tfrac{3}{2}U^2\chi(q)\left[\frac{1}{1-U\chi(q)}-1\right]+\tfrac{1}{2}U^2\chi(q)\left[\frac{1}{1+U\chi(q)}-1\right]\ , \tag{7}$$

with the polarizability

$$\chi(q)=-\int_k G(k+q)G(k)\ . \tag{8}$$

A number of techniques exist for the self-consistent solution of the preceding nonlinear integral equations. An alternative to the brute-force or fast-Fourier-transform techniques is a renormalization-group approach first investigated by Chen and Bickers in the context of parquet-equation solutions for the Anderson impurity model.[14] The central idea in the RG approach is the separation of a variable domain into "low" and "high" regions. For the 2D Hubbard model the initial variable domain is just the set of all k, i.e., the set of all Matsubara frequencies ω_n smaller in magnitude than a specified cutoff Ω and all wave vectors $\mathbf{k}$ within the square Brillouin zone. For convenience the low and high regions of the variable domain may be denoted L and H.

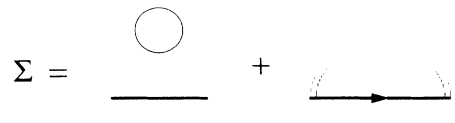

FIG. 1. Schematic representation of the one-electron self-energy Σ. Self-consistent Green's functions are denoted by solid lines, the basic interaction by a dashed line, and the effective potential V_{eff} by a double-dashed line. The first term is the Hartree correction, which may be eliminated by a redefinition of the chemical potential.

Suppose a function f on the variable domain is determined by an integral equation of the form

$$f(k)=\int_{k'}h(k,k')g(k')\ , \tag{9}$$

where g depends implicitly on the unknown function f. The FLEX equations written above take this form with $f\to\Sigma$, $h\to V$, and $g\to G$. The situation is slightly more complicated, however, since V *also* depends implicitly on the values of G and Σ throughout the entire space. We ignore this crucial point for the moment and return to it after developing a general technique for solving Eq. (9).

The integration in Eq. (9) may be broken into two parts as

$$f(k)=\int_{k'\in L}h(k,k')g(k')+\int_{k'\in H}h(k,k')g(k')\equiv\int_{k'\in L}h(k,k')g(k')+\Delta f(k)\ . \tag{10}$$

Clearly, if the function Δf were available from some other source, the labor of solving the integral equation would be greatly reduced: only an integration over L, rather than over the full space, would be required.

For calculations carried out at a sequence of decreasing temperatures, an iterative method for systematically dividing the variable domain and obtaining Δf may indeed be devised. The procedure is as follows.

(1) In the first stage, lay down a finite mesh which covers the initial variable domain. For a specified initial temperature T_0 this amounts to choosing a Matsubara cutoff Ω such that

$$\Omega_0=2N(T_0)\pi T_0 \tag{11}$$

for some integer $N(T_0)$ and dividing the square Brillouin zone $\{\mathbf{k}:-\pi<k_x\le\pi,\ -\pi<k_y\le\pi\}$ into a set of uniform squares centered on a finite set of $\mathbf{k}$ points. (Note that the fermion Matsubara frequencies automatically form a discrete set with $2N(T_0)$ elements spaced uniformly between $-[2N(T_0)-1]\pi T_0$ and $[2N(T_0)-1]\pi T_0$.)

(2) Solve integral equation (9) for the unknown function f within the discretized variable domain.

(3) Divide the variable domain into two parts L and H. The precise condition for the division determines the renormalization group to be employed. The simplest (and most useful) division of the frequency space amounts to the choice of a new cutoff Ω_1, which separates L and H. The most useful division of the momentum space invokes the concept of a Fermi surface S_F, with L consisting of wave vectors "close to" S_F and H the complement of L. Specific conditions for frequency- and momentum-space RG's are discussed at length in Secs. III A and III B.

(4) For discrete points k in L, calculate the contribution to $f(k)$ from points k' in H, i.e., explicitly compute

$$\Delta f(k)=\int_{k'\in H} h(k,k')g(k') \ . \tag{12}$$

(5) Choose a temperature $T_1 < T_0$ for a subsequent calculation of the unknown function f. The new temperature must be consistent with the new frequency cutoff Ω_1 (see Sec. III A).

(6) Lay down a new finite mesh covering the reduced space L. As in step (1), the choice of a temperature T_1 specifies a frequency mesh, which will be finer than the initial mesh since $T_1 < T_0$. The momentum space may also be regrained, e.g., by dividing each **k**-space square in L into four new squares, each centered on a new mesh point.

(7) Interpolate the function $\Delta f(k)$ determined in step (4) onto the new L mesh.

(8) Solve Eq. (10) within the reduced domain L using the *predetermined* function Δf from steps (4) and (7).

(9) Iterate steps (3)–(8) as desired to study additional temperatures and meshes. Note that the "renormalization correction" Δf obtained at temperature T_i is a sum of terms obtained from the previous i iterations.

The FLEX approximation may be solved using this technique ($\Delta f \rightarrow \Delta\Sigma$) with one important extension. The effective potential V_{eff} which enters Eq. (6) and plays the role of h in Eq. (9) is itself a functional of the one-electron Green's function (and hence the self-energy). For this reason it too must be renormalized in a stage-by-stage fashion. The necessary procedure is the analog of vertex renormalization in quantum field theory, just as the calculation of $\Delta\Sigma$ is the analog of mass and wave-function renormalization. For more general models this renormalization is nontrivial, since V_{eff} depends separately on the external variable k and the variable of integration k'. In the present case renormalization can be accomplished relatively simply, since V_{eff} depends only on the combination $k-k'$ through the polarizability χ defined in Eq. (8). Just as in the case of Σ, χ may be divided into contributions from the L and H regions of the variable domain:

$$\chi(q)=-\int_{k:k \text{ and } k+q\in L} G(k+q)G(k)+\Delta\chi(q) \ , \tag{13}$$

with

$$\Delta\chi(q)=-\int_{k:k \text{ or } k+q\in H} G(k+q)G(k) \ . \tag{14}$$

At each temperature the renormalization correction $\Delta\chi$ must be calculated along with $\Delta\Sigma$ and then interpolated onto the mesh to be used in the next RG stage [steps (4) and (7) of the preceding algorithm]. The calculation then proceeds as described above.[15]

The motivation of the RG procedure is clear: Accurate low-temperature calculations require the use of fine meshes in frequency and momentum space. The frequency discretization scale is inherently $\Delta\omega=2\pi T$, while the momentum discretization scale must also tend to zero if one is to resolve possible Fermi surface singularities in correlation functions. Nevertheless, brute-force calculations (and, to a lesser extent, FFT calculations) consume an enormous amount of time in computing functional contributions from regions of high frequency or momentum. One expects that such contributions invariably become temperature independent below some scale (which depends on the specific frequency or momentum in question). By carrying out a series of calculations on meshes of increasing magnification in domains of decreasing size, the total labor required to solve a problem may be enormously reduced. In some cases the total calculational time to reach a temperature T using the RG approach scales as $|\ln T|$, rather than as T^{-2} (brute-force approach) or $T^{-1}|\ln T|$ (FFT approach).

In order for the FLEX RG procedure to work, the contribution to $\Delta\Sigma$ from a given domain H must (a) be nearly independent of temperature for all temperatures below the scale at which it is actually calculated and (b) vary smoothly on the scale of the mesh for which it is calculated. The first condition is essential since once a domain H is eliminated, it appears at no subsequent stage (i.e., lower temperature) in a calculation. The second condition is also important since any useful RG sequence introduces meshes of increasing magnification, for which interpolation is required. By renormalizing sufficiently slowly (i.e., by choosing L sufficiently close to the initial variable domain), both conditions may be satisfied. As shown in Sec. IV, accuracy at the 1% level may be obtained using surprisingly large RG steps, with improvements in efficiency of several *orders of magnitude* at low temperature. Such accuracy is completely acceptable for thermodynamic applications and for a limited range of dynamic applications as well.[16]

A. Frequency-space renormalization group

In general the FLEX equations for a 2D system may be solved using (a) a frequency-space RG with fixed momentum discretization, (b) a momentum-space RG with fixed frequency discretization (and fixed temperature), or (c) a general RG which eliminates regions of frequency and momentum space concurrently. We have found it sufficient to use composite RG's based on alternating stages of (a) and (b) in order to reach very low temperatures. For this reason we treat cases (a) and (b) separately, beginning in this section with a discussion of frequency-space RG's.

A frequency-space RG sequence may be defined by choosing a set of temperatures T_i and frequency cutoffs Ω_i such that

$$T_0 > T_1 > T_2 > \cdots \tag{15}$$

and

$$\Omega_0 \geq \Omega_1 \geq \Omega_2 \geq \cdots \ . \tag{16}$$

These quantities cannot be chosen at random, but must satisfy several conditions discussed below. The total number of positive fermion Matsubara frequencies in the initial stage of the calculation can be denoted $N(T_0)$. This number defines the frequency cutoff Ω_0 through Eq. (11). This initial cutoff must be chosen sufficiently large that calculated quantities are cutoff independent.

The cutoffs and temperatures for subsequent RG stages

must satisfy the conditions

$$\Omega_i = 2N(T_i)\pi T_i \tag{17}$$

and

$$\Omega_i = 2K(T_i)\pi T_{i-1} \tag{18}$$

for some integers $N(T_i)$ and $K(T_i)$ such that

$$1 \le K(T_i) \le N(T_{i-1}) \ . \tag{19}$$

Both conditions are essential if the RG is to be length preserving on the imaginary frequency axis. The total length of the initial frequency domain is

$$2\pi T_0 \sum_{\omega_n(T_0)} 1 = 2\pi T_0[2N(T_0)] = 2\Omega_0 \ . \tag{20}$$

After the first RG division into L and H, this total length can be rewritten as

$$2\pi T_1 \sum_{\omega_n(T_1)\in L} 1 + \Delta f = 2\pi T_1[2N(T_1)] + \Delta f$$
$$= 2\pi T_0[2K(T_1)] + \Delta f \ , \tag{21}$$

where

$$\Delta f = 2\pi T_0 \sum_{\omega_n(T_0)\in H} 1 = 2\pi T_0[2N(T_0) - 2K(T_1)] \ . \tag{22}$$

The total length of the original frequency interval is preserved. This is insured by requiring that the cutoffs coincide exactly with boson Matsubara frequencies: If this were not true, the length of the original frequency domain could not be reproduced exactly by repeated RG iterations, and more complicated summations would also be distorted.

As shown in Sec. IV, a convenient choice for rapid renormalization is

$$K(T_i)/N(T_i) = T_i/T_{i-1} = \tfrac{1}{2} \ ,$$
$$K(T_i)/N(T_{i-1}) = \Omega_i/\Omega_{i-1} = \tfrac{1}{2} \tag{23}$$

for $i = 1, 2, \ldots$. This amounts to simultaneous reduction of the temperature scale and the frequency cutoff by a factor of 2 at each RG stage [see Fig. 2(a)]. The total number of fermion frequencies employed in each stage is then the same as the number employed in the first stage, i.e., $2N(T_0)$. This means that if the number of iterations to reach convergence remains constant from stage to stage, each stage takes exactly the same calculational time. The total calculational time to pass from a temperature T_0 to a temperature $T_N = 2^{-N}T_0$ is then just $N+1$ times the calculational time for temperature T_0. This logarithmic scaling with T_N should be compared with the performance of brute-force (time $\propto T_N^{-2}$) or FFT (time $\propto T_N^{-1}|\ln T_N|$) algorithms. (In fact, the number of iterations to reach convergence at a single stage slowly increases as the temperature decreases. Since this is true for each type of algorithm, it does not alter the basic comparison of efficiencies.)

While rapid renormalization is the key to calculational efficiency, it may in some cases be necessary to scan slowly through a specified temperature range. For example, a slow scan may be preferable in the vicinity of a phase transition, where one or more susceptibilities exhibit power-law divergences. The simplest way to accomplish a slow scan is to keep the cutoff *fixed* while slowly decreasing the temperature, i.e., to set

$$K(T_i) = N(T_{i-1}) \ , \tag{24}$$

with $N(T_i)$ a slowly increasing integer function of i. [For a pictorial illustration of this process, see Fig. 2(b).] The temperatures T_i satisfy the relation

$$T_i = \frac{K(T_i)}{N(T_i)} T_{i-1} \ . \tag{25}$$

After scanning the temperature range of interest, more rapid renormalization can again be introduced.

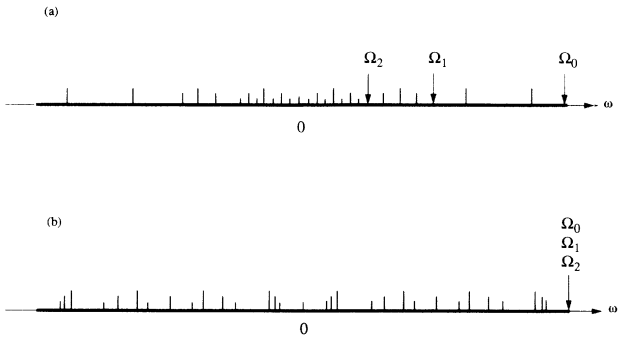

FIG. 2. Imaginary frequency discretization for two frequency-space renormalization groups: (a) Initial three stages of the "factor-of-2" RG. The cutoffs Ω_0, Ω_1, and Ω_2 are represented by arrows. Four positive and four negative fermion frequencies appear for each cutoff. The fermion frequencies are represented by tick marks of varying length, the longest for $i=0$ and the shortest for $i=2$. (b) Initial three stages of "constant-cutoff" RG with $N(T_0)=4$, $N(T_1)=5$, and $N(T_2)=6$. In this case there is effectively no renormalization, since the entire space is retained as L (i.e., H is the null set). As in (a), fermion frequencies are represented by tick marks, the longest for $i=0$ and the shortest for $i=2$.

B. Momentum-space renormalization group

In order to obtain accurate correlation functions at low temperatures, a fine discretization of momentum space is generally required. This is particularly true in the vicinity of the Fermi surface. A momentum-space RG may be devised in order to carry out integrations over all parts of the Brillouin zone efficiently.

Our basic $\mathbf{k}$-space integration algorithm is as follows: Cover the Brillouin zone $\{\mathbf{k}: -\pi < k_x \le \pi, \ -\pi < k_y \le \pi\}$ with a set of squares, centered on points $\mathbf{k}_i$ with area A_i; then estimate a $\mathbf{k}$-space integral as

$$\int_{-\pi}^{\pi} \frac{dk_x}{2\pi} \int_{-\pi}^{\pi} \frac{dk_y}{2\pi} f(\mathbf{k}) \simeq (2\pi)^{-2} \sum_i f(\mathbf{k}_i) A_i \ . \tag{26}$$

Once an initial discretization is specified (e.g., a uniform 4×4 breakup for high temperatures), it is necessary

to develop a method for dividing the momentum space into L and H. In the imaginary-frequency domain a simple division into low and high frequencies separated by a cutoff is possible. In the present case the important variable is distance from the Fermi surface. Two Fermi surfaces come to mind for a system with fixed electron filling $\langle n \rangle$: the noninteracting Fermi surface with chemical potential μ_0 and the interacting Fermi surface with chemical potential μ. While the locus of points defining the Fermi surface in $\mathbf{k}$ space is expected to change only slightly when interactions are turned on, the value of the chemical potential may change significantly.

The simplest measure of distance from the Fermi surface in a noninteracting system is the energy $\varepsilon_{\mathbf{k}}-\mu_0$. (If the Fermi surface were spherical, the distance $|\mathbf{k}-k_F\hat{k}|$ would also be a convenient variable. In lattice systems the Fermi surface is never precisely spherical, and the perpendicular distance is difficult to compute.) This energy variable could be used as the basis for an RG even in an interacting system, but difficulties would likely arise at low temperatures where the interacting and noninteracting Fermi surfaces differ slightly in shape. We have found it more convenient to use an energy variable based directly on the interacting system, namely,

$$\xi_{\mathbf{k}}(T)\equiv(\varepsilon_{\mathbf{k}}-\mu)+\mathrm{Re}\Sigma(\mathbf{k},i\pi T) . \tag{27}$$

For $T\rightarrow 0$, this variable should vanish precisely on the interacting Fermi surface.

A reasonable condition for splitting the momentum space into L and H regions is

$$\begin{aligned} &|\xi_{\mathbf{k}}(T)|>\Omega^K \Longrightarrow \mathbf{k}\in H , \\ &|\xi_{\mathbf{k}}(T)|\leq\Omega^K \Longrightarrow \mathbf{k}\in L , \end{aligned} \tag{28}$$

with Ω^K a suitably chosen cutoff energy. An accurate RG requires the choice of a sequence of cutoffs Ω_i^K which do not decrease too rapidly.

The accuracy of results from a particular choice of Ω^K may always be gauged directly by repeating a calculation without reducing the $\mathbf{k}$ space from the previous stage. However, since the momentum-space RG will, in practice, always be used in combination with a frequency-space RG, it is useful to obtain a rough correspondence between Ω_i^K and the current value of the frequency cutoff Ω_i. Such a correspondence can be obtained by examining the form of the one-electron Green's function. The Green's function may be written

$$\begin{aligned} G(\mathbf{k},i\omega_n)&=[i\omega_n-(\varepsilon_{\mathbf{k}}-\mu)-\Sigma(\mathbf{k},i\omega_n)]^{-1} \\ &=[Z(\mathbf{k},i\omega_n)(i\omega_n)-\xi(\mathbf{k},i\omega_n)]^{-1} , \end{aligned} \tag{29}$$

where

$$\begin{aligned} Z(\mathbf{k},i\omega_n)&=1-\frac{\mathrm{Im}\Sigma(\mathbf{k},i\omega_n)}{\omega_n} , \\ \xi(\mathbf{k},i\omega_n)&=(\varepsilon_{\mathbf{k}}-\mu)+\mathrm{Re}\Sigma(\mathbf{k},i\omega_n) . \end{aligned} \tag{30}$$

In terms of the Green's function, the success of the frequency-space RG depends on the appearance of large energy denominators in the H region. The energy denominators have an imaginary part $Z(\mathbf{k},i\omega_n)\omega_n$ and a real part $\xi(\mathbf{k},i\omega_n)$. If the RG condition

$$\begin{aligned} &|\omega_n|>\Omega \Longrightarrow \omega_n\in H , \\ &|\omega_n|\leq\Omega \Longrightarrow \omega_n\in L \end{aligned} \tag{31}$$

is successful (i.e., leads to acceptably small errors), then a comparable momentum-space division can be devised using the correspondence between $Z(\mathbf{k},i\omega_n)\omega_n$ and $\xi(\mathbf{k},i\omega_n)$. Let $\tilde{Z}$ be a typical value of $Z(\mathbf{k},i\omega_n)$ in the *frequency-space* H region (so that $|\omega_n|>\Omega$). Then the choice

$$\Omega^K=\tilde{Z}\Omega \tag{32}$$

for a momentum-space RG condition should lead to errors comparable in magnitude to those from the frequency-space division based on Ω. In many cases, $\tilde{Z}$ turns out to be no larger than 2 or 3 (particularly in the early stages of a calculation); since Eq. (32) only gives order-of-magnitude estimates, it is then sufficient to just set $\Omega^K\simeq\Omega$.[17]

Once a choice has been made for the cutoff Ω^K, the discretized momentum space may be divided. Our convention is that a momentum square labeled by i falls entirely within L or H depending upon the condition satisfied by its center point $\mathbf{k}_i$. If a square falls within L, it must be rediscretized for the next RG stage. In contrast with our treatment of imaginary frequencies, for which the discretization scale is automatically set by the temperature, we only allow two possible rediscretizations of momenta: (1) a 2×2 division of each square into uniform smaller squares, each centered at a new point $\mathbf{k}_i$, or (2) no rescaling, i.e., an identity operation. The amount

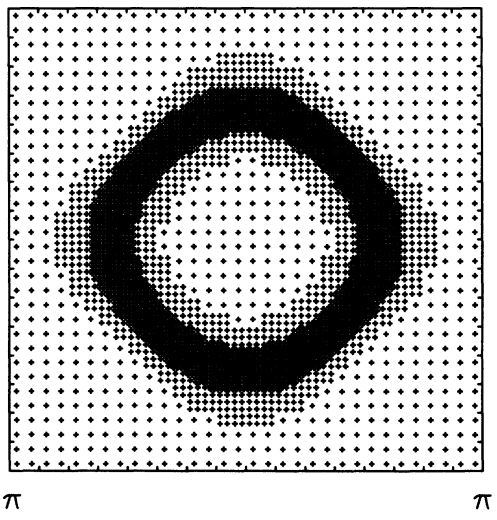

FIG. 3. Brillouin-zone discretization for a sample momentum-space renormalization group. Three stages are illustrated. The initial mesh has 32^2 points, while the next two meshes have reduced areas, with scales corresponding to 64^2 and 128^2 points within the full zone. The cuts were made for the FLEX approximation with $U/t=8$ and $\mu/t=-3$, corresponding to filling $\langle n \rangle=0.53$ at zero temperature. The energy cutoffs are $\Omega_1^K/t=1.51$ and $\Omega_2^K/t=0.76$.

of work required at the next RG stage depends on the number of rediscretized squares in L. If no rescaling occurs, the work will be reduced in comparison with the current stage; if a 2×2 rescaling occurs, the work may be either reduced or increased depending on the number of squares dropped in the H region.

Note that the boundary between the L and H regions in our approach is composed entirely of straight-line segments, since our elements of integration are always squares. Figure 3 shows a typical momentum-space RG discretization starting from a 32^2 mesh and ending with a 128^2 mesh. The emergence of a Fermi surface (i.e., a one-dimensional curve within the two-dimensional Brillouin zone) is graphically illustrated.

IV. RESULTS

In this section we examine results for one-electron self-energies, Green's functions, occupancy factors, and instability eigenvalues obtained using a variety of different RG's. Our principal conclusion is that RG methods can be used in high-accuracy imaginary-frequency calculations at a small fraction of the labor required for more conventional approaches. We will compare results obtained by the RG approach and by a straightforward brute-force solution of the FLEX equations. For the simplest Hubbard model considered here, the most efficient alternative to the RG is not the brute-force solution, but an FFT technique relying on the appearance of convolution integrals in FLEX. While time requirements for the brute-force technique scale as N^2, with N the total number of $(\mathbf{k},i\omega_n)$ points, time requirements for the FFT technique scale only as $N\ln N$. This should be taken into account in interpreting efficiencies for this particular model: The RG approach is more efficient than the FFT-based solution by an amount which scales asymptotically as T^{-1}, rather than as T^{-2}. In more general problems (viz., those in which the effective potential $V_{\rm eff}$ depends separately on the external and internal momentum variables k and k', rather than on their difference), the FFT approach is not applicable. In such cases the only solution techniques we know of are a brute-force solution and an RG approach (somewhat more complex than the approach used here). The time comparisons generated below for the Hubbard model are also indicative of the RG's potential advantage in these cases.

To begin with, we examine the accuracy and efficiency of a frequency-space RG for a fixed momentum-space mesh. Results are shown in Fig. 4 for a 16^2 mesh at a generic filling $\langle n\rangle=0.87$. The Coulomb energy is $U/t=7$ and the temperature $T/t=0.03$. Results for the real and imaginary parts of the self-energy [Fig. 4(a)] and the Green's function [Fig. 4(b)] were obtained using a brute-force solution of the FLEX equations (solid lines) and a frequency-space RG in which the temperature and cutoff were reduced by a factor of 2 at each stage (symbols). Both calculations assume an initial frequency cutoff $\Omega_0/t=25$, and the RG calculation proceeds from stages $i=0$ to 5 with a constant number of positive fermion frequencies $N(T_i)=4$ at each stage. The results are in agreement in the 2–4 % level for the self-energy, and at the 1% level for the Green's function. The calculational time per convergence iteration for the brute-force approach is 1800 Sun-400 CPU sec, while the time for the RG approach is only 6 sec, a savings of a factor of 300. The total storage required for the brute-force calculation is 0.4 Mbytes, while the storage for the RG approach is 0.03 Mbytes, a savings of a factor of 13. The advantage of the RG approach continues to improve as the temperature is lowered: Eventually, the brute-force solution be-

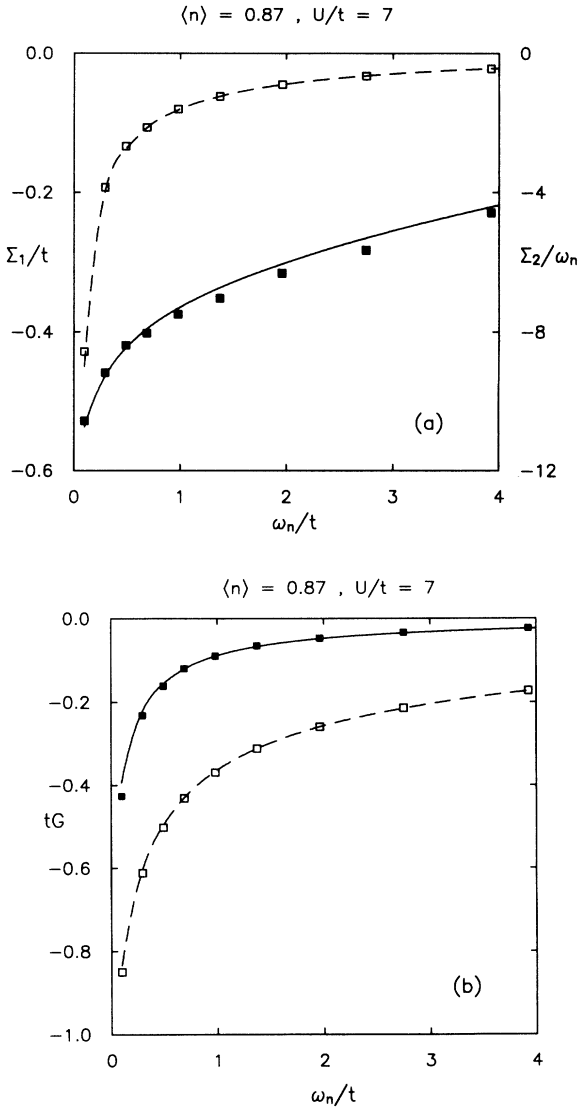

FIG. 4. Comparison of self-energies $\Sigma_1+i\Sigma_2$ and Green's functions G_1+iG_2 obtained using the factor-of-2 frequency-space RG and a brute-force approach. The model parameters are $U/t=7$ and $\langle n\rangle=0.87$, and the $\mathbf{k}$-space mesh has 16^2 points. The temperature is $T/t=0.03$. The selected $\mathbf{k}$ point is $\mathbf{k}=(2.95,0.20)$. Results from the five-stage RG are represented by symbols, and results from the brute-force calculation by lines. (a) Real (solid squares and line) and imaginary (open squares and dashed line) parts of the self-energy. Note that Σ_2/ω_n, rather than Σ_2/t, is plotted (Ref. 15). (b) Real (solid squares and line) and imaginary (open squares and dashed line) parts of the Green's function.

comes completely impractical, while each new stage of the RG calculation requires roughly the same time as the preceding stage [because $N(T_i)$ is fixed].

Although our main intent in this paper is to emphasize the development of the RG approach, it is perhaps useful at this point to comment on the functional form of the self-energy in Fig. 4(a). The low-frequency asymptotic form expected for conventional Fermi liquid behavior in two dimensions is (for $\omega_n > 0$)

$$\Sigma(\mathbf{k}_F, i\omega_n; T\to 0) \sim \Sigma_0 + (1-Z_0)(i\omega_n) + i\gamma(i\omega_n)^2 \ln(i\omega_n/\omega_0) , \tag{33}$$

where Σ_0, Z_0, and ω_0 are real valued and $\gamma \equiv \gamma_1 + i\gamma_2$ is complex, with $\gamma_1 > 0$. This function analytically continues to

$$\Sigma(\mathbf{k}_F, \omega + i0^+; T\to 0) \sim (1-Z_0)\omega + i\gamma\omega^2 \ln|\omega/\omega_0| - \pi\gamma\omega^2\theta(-\omega) \tag{34}$$

on the real axis. The predicted Fermi liquid behavior of Σ_1 and Σ_2/ω_n is (for $\omega_n > 0$)

$$\begin{aligned} &\Sigma_1(i\omega_n) \sim \Sigma_0 + \gamma_2\omega_n^2 \ln|\omega_n/\omega_0| + \tfrac{1}{2}\pi\gamma_1\omega_n^2 , \\ &\Sigma_2(i\omega_n)/\omega_n \sim (1-Z_0) - \gamma_1\omega_n \ln|\omega_n/\omega_0| + \tfrac{1}{2}\pi\gamma_2\omega_n . \end{aligned} \tag{35}$$

The function in Fig. 4(a) *cannot* be adequately fit to the form in Eq. (35) within the range of frequencies and temperatures studied. On the other hand, it can be fit quite well by the assumed dependence

$$\begin{aligned} &\Sigma(i\omega_n) = \Sigma_0 + \Gamma(i\omega_n)^\alpha + (1-Z_0)(i\omega_n) , \\ &\Gamma = \Gamma_1 + i\Gamma_2 , \end{aligned} \tag{36}$$

i.e.,

$$\begin{aligned} &\Sigma_1(i\omega_n) = \Sigma_0 + [\Gamma_1\cos(\alpha\pi/2) - \Gamma_2\sin(\alpha\pi/2)]|\omega_n|^\alpha , \\ &\Sigma_2(i\omega_n)/\omega_n = [\Gamma_2\cos(\alpha\pi/2) + \Gamma_1\sin(\alpha\pi/2)]|\omega_n|^{\alpha-1} + (1-Z_0) , \end{aligned} \tag{37}$$

where $\alpha < 1$. This is the simplest analytic functional form consistent with a *violation* of Fermi liquid behavior. Note that the same noninteger exponent α must be common to both the real and imaginary parts of the self-energy.

The parameters which follow from a nonlinear least-squares fit to the RG data in Fig. 4(a) are $\alpha = 0.24 \pm 0.01$, $\Gamma = -0.2 - 1.5i$, $\Sigma_0 = -0.73$, and $Z_0 = 1.2$. This analysis provides strong evidence that the FLEX approximation yields non-Fermi liquid behavior for a *range* of electron fillings near $\langle n \rangle = 1$ when the Coulomb energy U/t is made sufficiently large. Serene and Hess[6] have established previously the existence of non-Fermi liquid behavior at half-filling even for weak U/t, and the absence of such behavior at quarter filling for $U/t = 8$. The results above do not contradict these findings: The singular behavior of Σ in Fig. 4(a) is due to the presence of a highly singular effective interaction induced by the exchange of spin fluctuations. For sufficiently weak U/t and $\langle n \rangle \neq 1$, V_{eff} would remain bounded for $T\to 0$, since the noninteracting density of states is nonsingular (i.e., the lattice is not perfectly nested). In the present case, U/t is large enough to cause a divergence in V_{eff} for $T\to 0$ and a related singularity in the self-energy. The implications of this result are difficult to gauge for several reasons: First, the FLEX approximation need not yield the same result as an exact solution. Second, the singularity appears in a normal-state solution, which will generally be preempted as low temperature by a broken symmetry solution of lower free energy (an anisotropic superconducting state in the present approximation). Despite these caveats, the appearance of non-Fermi liquid behavior in the analysis of a microscopic model is of considerable interest. This subject is addressed at length in a separate article.

At this point we return to our analysis of the RG solution technique. The factor-of-2 frequency-space RG introduced previously is used in most of the figures which follow. Some freedom remains in choosing the constant $N(T_i)$, the number of positive fermion frequencies at each stage. Note that in a brute-force (or FFT) calculation this number is $\Omega_0/2\pi T_i$, i.e., it grows as T_i^{-1}. In Fig. 5 results are shown for the self-energy and Green's function calculated using the factor-of-2 RG with the choices $N(T_i) = 2$, 4, and 8. The model parameters are $U/t = 8$ and $\langle n \rangle = 0.53$, and the temperature $T/t = 0.0075$. The initial frequency cutoff is $\Omega_0/t = 96$, and a 32^2 Brillouin-zone discretization is employed. (This fine discretization allows a choice of $\mathbf{k}$ very close to the Fermi surface, where the Green's function is most sensitive to small errors in the self-energy.) The real and imaginary parts of the self-energy [Figs. 5(a) and 5(b)] and Green's function [Figs. 5(c) and 5(d)] are shown for $\mathbf{k} = (1.18, 1.18)$, just below the Fermi surface along the Brillouin-zone diagonal. (It is interesting to note in passing that, as concluded previously by Serene and Hess,[6] the self-energy exhibits conventional Fermi liquid behavior in this range of filling and interaction strength.)

Clearly, the RG cannot be expected to remain accurate if $N(T_i)$ is made too small. In fact, the results for $N(T_i) = 2$ are surprisingly accurate at high frequencies (or temperatures; not illustrated here). The results for $N(T_i) = 4$ and 8 are nearly the same at all temperatures, illustrating rapid saturation to the $N\to\infty$ limit. In the plots which follow we choose $N(T_i) = 4$, which allows a stage-by-stage savings over $N(T_i) = 8$ of roughly a factor of 2 in storage and 4 in calculation time. As a reference point, the calculation described above (with no momentum-space RG improvement) requires 90 CPU sec per convergence iteration for $N(T_i) = 4$ on a Sun-400 workstation. A speed increase by a factor of 40 can be obtained using a Cray Y-MP. The corresponding brute-force calculation would be completely impractical: the required value of $N(T_i)$ rises to $\Omega_0/2\pi T_i = 2000$, giving a calculation time per iteration of

$$(2000/8)^2(240) \text{ CPU sec} = 4200 \text{ CPU h} .$$

As an illustration of the frequency-space RG's use in computing a simple thermodynamic function, Fig. 6 shows results for the momentum-space occupancy factor $n_{\mathbf{k}}(T)$ [Fig. 6(b)], computed along a triangular Brillouin-

zone contour [Fig. 6(a)]. The occupancy factor is just an equal-time Green's function:

$$n_{\mathbf{k}}(T)=2G(\mathbf{k},\tau\to 0^-)=2T\sum_{n=-\infty}^{\infty} e^{i\omega_n 0^-}G(\mathbf{k},i\omega_n)$$

$$\simeq 1+2T\sum_{|\omega_n|<\Omega_0} G(\mathbf{k},i\omega_n)\ . \quad (38)$$

Like any time-dependent correlation function, the occupancy factor has contributions from *all* frequency scales. For this reason, its RG representation at temperature T_M takes the form

$$n_{\mathbf{k}}(T_M)=1+\sum_{j=0}^{M} 2T_j \sum_{\Omega_{j+1}<|\omega_n(T_j)|<\Omega_j} G(\mathbf{k},i\omega_n)\ , \quad (39)$$

with

$$\Omega_{M+1}\equiv 0\ . \quad (40)$$

The results in Fig. 6(b) are for $U/t=8$, $\langle n\rangle=0.53$, and $T/t=0.0075$, with an initial cutoff $\Omega_0/t=96$. Brillouin-zone discretizations of 16^2 (squares), 32^2 (circles), and 64^2 points (solid line) were employed. All calculations were performed on a Sun-400 workstation (for which the brute-force approach at this low temperature is unfeasible). The results for the 32^2 and 64^2 discretizations are essentially identical at this temperature, but show significant deviations from the 16^2 results near the Fermi surface. To study the shape of the occupancy factor at even lower temperatures, it is convenient to introduce a momentum-space RG, as discussed below.

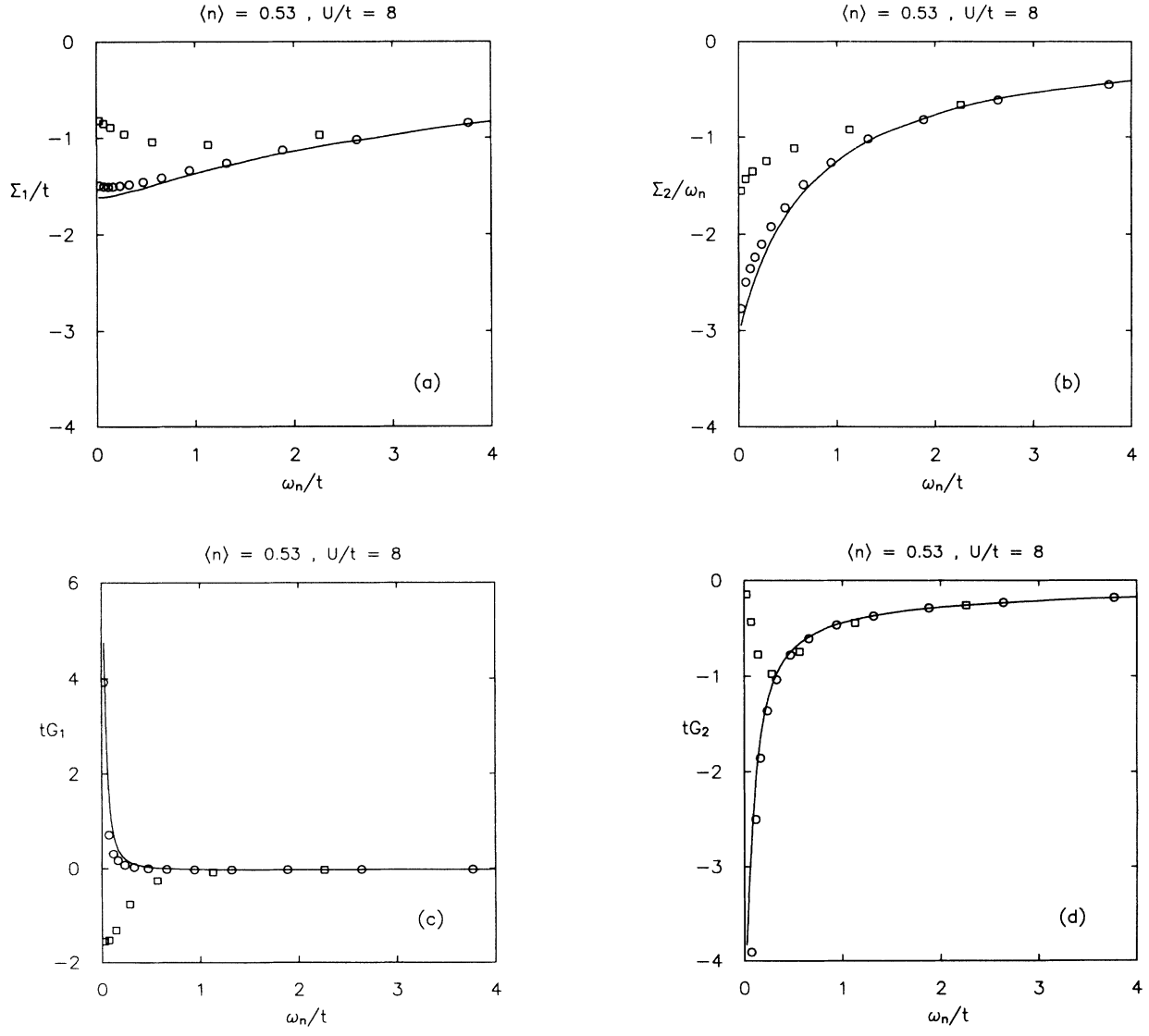

FIG. 5. Comparison of results from the factor-of-2 frequency-space RG with varying $N(T_i)$. Results are shown for $N(T_i)=2$ (squares), 4 (circles), and 8 (solid lines). The model parameters are $U/t=8$ and $\langle n\rangle=0.53$, and the temperature is $T/t=0.0075$. The self-energy $\Sigma_1+i\Sigma_2$ and Green's function G_1+iG_2 are plotted for the point $\mathbf{k}=(1.18,1.18)$. (a) Σ_1/t; (b) Σ_2/ω_n; (c) tG_1; (d) tG_2.

The sequential elimination of high momenta is conceptually as easy as the elimination of high frequencies. Care must be taken, however, not to eliminate momenta too rapidly, as noted in Sec. III B. Results are shown in Fig. 7 for the self-energy and Green's function at a single $\mathbf{k}$ point [$\mathbf{k}=(1.33,1.33)$] for a range of temperatures. The $\mathbf{k}$ point is chosen to be close to the potential dividing line between L and H regions of momentum space. As in Fig. 5, $U/t=8$ and $\langle n\rangle=0.53$. The temperatures are $T/t=0.06$ (squares), 0.03 (circles), and 0.015 (lines). The factor-of-2 frequency-space RG was employed with $\Omega_0/t=96$, and the Brillouin-zone discretization is fixed at 64^2. At low frequencies the results for $T/t=0.06$ and 0.03 vary by significant amounts [roughly 10% for the imaginary part of the self-energy in Fig. 7(a)]. On the other hand, the results for $T/t=0.03$ and 0.015 are nearly identical. This indicates that any momentum-space RG which eliminates the point $\mathbf{k}=(1.33,1.33)$ at temperatures above $T/t=0.03$ tends to introduce errors of several percent. The value of $\xi_{\mathbf{k}}(T)/t$ is in this case about 0.58. The value of the cutoff Ω/t for $T/t=0.06$ is 1.51. The corresponding momentum-space cutoff Ω^K for this stage should be at least as big. This is larger than $\xi_{\mathbf{k}}(T)$, indicating that $\mathbf{k}$ should definitely be retained at this stage. On the other hand, at $T/t=0.015$, the value of Ω/t is 0.38. In this case, $\Omega^K\simeq\Omega$ is smaller than $\xi_{\mathbf{k}}(T)$, indicating that $\mathbf{k}$ is a candidate for elimination at this temperature. [If Eq. (32) is strictly applied as a criterion, $\mathbf{k}$ would be retained for one additional stage.)

The dependence of results on the choice of Ω^K is illustrated directly in Fig. 8. The parameter choice is as in Fig. 7, the $\mathbf{k}$ point is chosen as above, and $T/t=0.015$. The results were obtained using two different RG procedures: the factor-of-2 frequency-space RG on a fixed 64^2 mesh (lines) and a combined frequency+momentum-space RG (symbols). The latter procedures employs the frequency-space RG to reach $T/t=0.03$ on a 32^2 mesh,

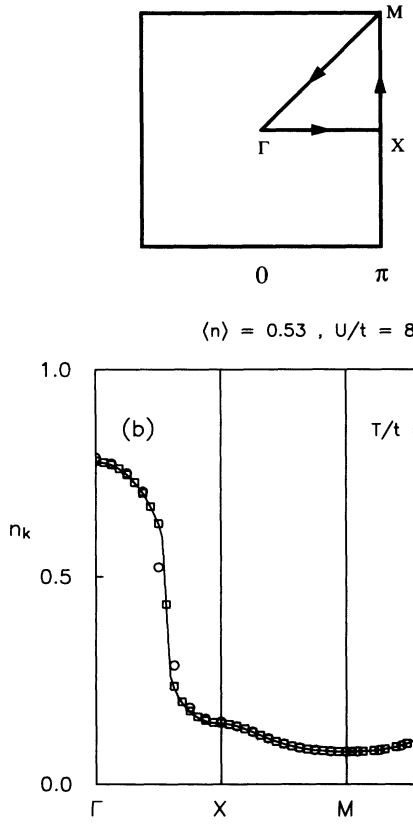

FIG. 6. Calculation of the occupancy factor $n_{\mathbf{k}}$ by the factor-of-2 frequency-space RG: (a) Triangular Brillouin-zone contour for plotting $n_{\mathbf{k}}$. (b) Occupancy factor for $U/t=8$ and $\langle n\rangle=0.53$ at temperature $T/t=0.0075$. Results are shown for Brillouin-zone discretizations with 16^2 (circles), 32^2 (squares), and 64^2 (line) points.

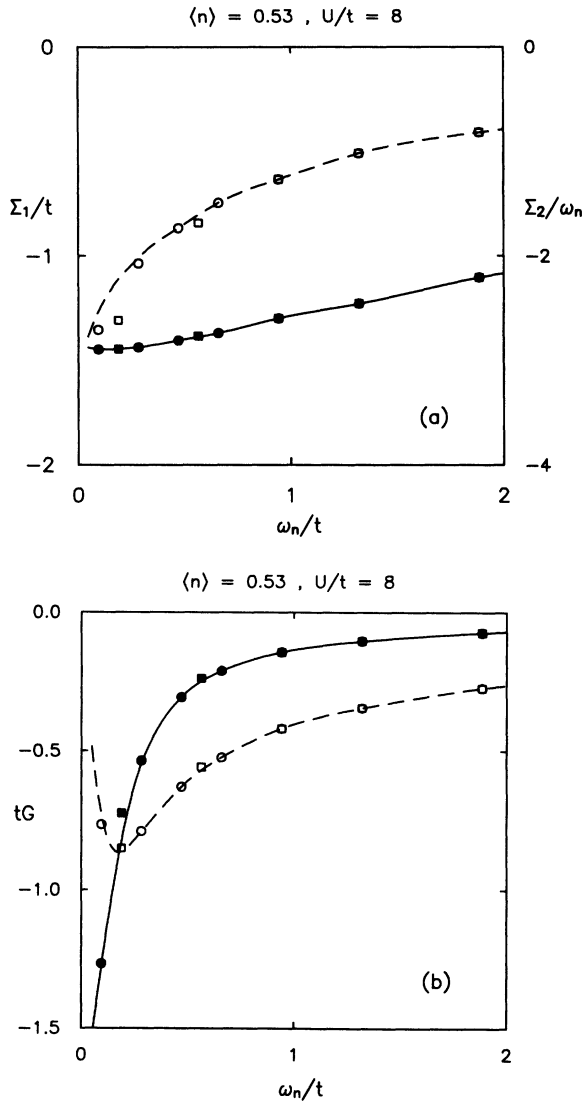

FIG. 7. Accuracy test for implementation of the momentum-space RG. The self-energy and Green's function at a point $\mathbf{k}=(1.33,1.33)$, just outside an L-region boundary, are plotted for three different temperatures. The model parameters are $U/t=8$ and $\langle n\rangle=0.53$. The temperatures are $T/t=0.06$ (squares), 0.03 (circles), and 0.015 (lines). (a) Real and imaginary parts of the self-energy, Σ_1/t (solid symbols and line) and Σ_2/ω_n (open symbols and dashed line). (b) Real and imaginary parts of the Green's function tG_1 (solid symbols and line) and tG_2 (open symbols and dashed line).

reduces the momentum space as described above, then rediscretizes to a 64^2 mesh, and finally employs the frequency-space RG one last time to reach $T/t=0.015$. This procedure has been carried out for three different choices of Ω^K/t: 0.76 (squares), 1.51 (circles), and 3.02 (triangles). The first choice corresponds to $\Omega^K=\Omega$ at $T/t=0.03$, and the other choices are more conservative. The only significant error from a small cutoff appears in the low-frequency quantity $\mathrm{Im}\Sigma(\mathbf{k},\pi T)/\pi T$. Note, however, that the absolute error in $\mathrm{Im}\Sigma$ remains acceptably small even at this point and that the percentage error in the Green's function $\Delta G/|G|$ is of order 1–2 % even for $\Omega^K/t=0.76$.

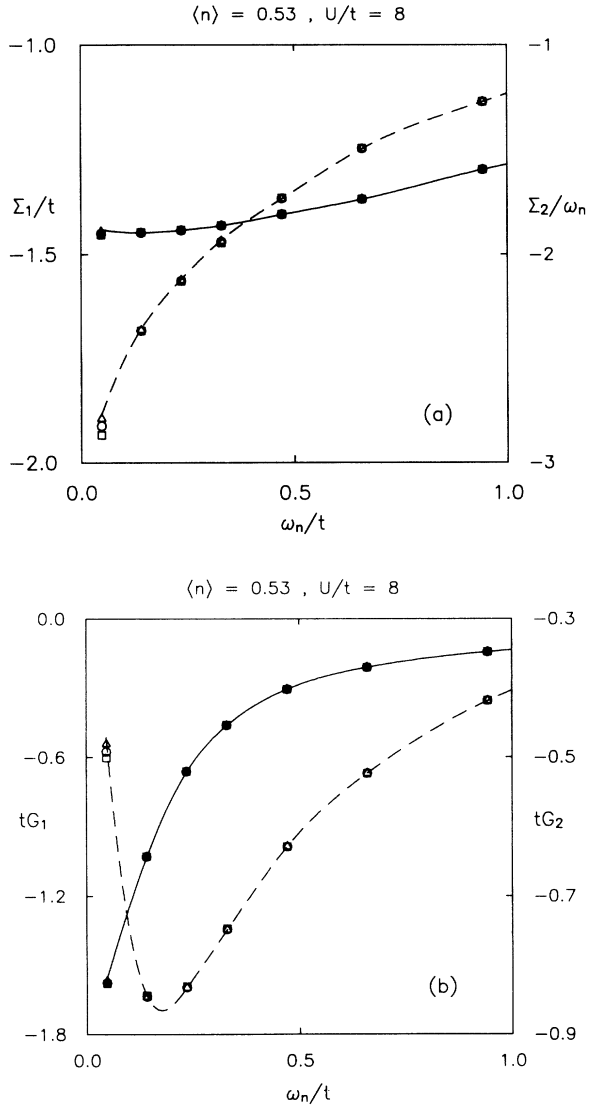

FIG. 8. Sensitivity of results to varying choices of the momentum-space energy cutoff Ω^K. Model parameters are as in Fig. 7, and the temperature is $T/t=0.015$. The **k** point is also chosen as in Fig. 7. Results are shown for a 64^2 mesh within the full Brillouin zone (lines) and for reduced **k**-space meshes with cutoffs of $\Omega^K/t=0.76$ (squares), 1.51 (circles), and 3.02 (triangles). (a) Real (solid line and symbols) and imaginary (dashed line and open symbols) parts of the self-energy. (b) Real (solid line and symbols) and imaginary (dashed line and open symbols) parts of the Green's function.

Results for the occupancy factor $n_{\mathbf{k}}(T)$ from the combined frequency+momentum-space RG are shown in Fig. 9. The model parameters are $U/t=8$ and $\langle n\rangle=0.53$, with an initial frequency cutoff $\Omega_0/t=96$. Two calculations are illustrated, both using the factor-of-2 frequency-space RG to reach a final temperature of $T/t=0.0075$. The first (squares) employs a 32^2 discretization at *all* temperatures. The second (circles and inset) begins with a 32^2 discretization and then applies a set of momentum-space RG operations to reach an effective mesh size of 512^2 near the Fermi surface. Note that at $T/t=0.0075$, a 32^2 mesh is completely sufficient to eliminate finite discretization effects, as shown in Fig. 6: The purpose of further magnification is to obtain a sample test of the momentum-space RG's accuracy and time and storage requirements. The ability to magnify near the Fermi surface is essential, however, in problems with Fermi surface singularities (as illustrated subsequently).

The combined set of frequency+momentum-space RG operations for Fig. 9 is as follows: (1) A 32^2 mesh is employed at the outset, and the frequency-space RG is iterated seven times, from $T_0/t=3.84$ down to $T_7/t=0.03$; (2) the momentum space is reduced at fixed temperature $T_7/t=0.03$ by introducing $\Omega^K/t=0.75$ and then rediscretizing the resulting L region with a 64^2 mesh; (3) the frequency-space RG is applied to reach a

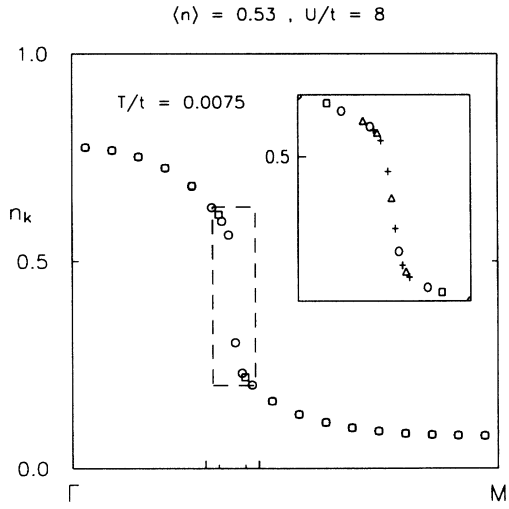

FIG. 9. Results for the occupancy factor $n_{\mathbf{k}}$ from a combined frequency+momentum-space RG. The model parameters are $U/t=8$ and $\langle n\rangle=0.53$, with temperature $T/t=0.0075$. The squares were obtained using the factor-of-2 frequency-space RG on a fixed 32^2 mesh. The circles were obtained by a combined set of frequency- and momentum-space operations to reach an effective 128^2 mesh near the Fermi surface. Regions of magnification are represented by tick marks on the ΓM axis: The outermost region is 32^2, then comes a narrow band of 64^2, and, finally, the 128^2 region. The boxed portion of the plot is further magnified in the inset, where two additional momentum-space operations at fixed temperature carry the mesh scale to 256^2 (triangles) and, finally, 512^2 (crosses).

temperature $T_8/t=0.015$; (4) the momentum space is again reduced at fixed temperature, this time with $\Omega^K/t=0.38$ and a 128^2 rediscretization; (5) the frequency-space RG is applied to reach the final temperature $T_9/t=0.0075$; and (6) the momentum space is reduced twice more at fixed temperature, first using $\Omega^K/t=0.19$ and rediscretizing to a 256^2 mesh, and then using $\Omega^K/t=0.15$ and rediscretizing to a 512^2 mesh. (Note that there would be no difficulty in passing to even lower temperatures via the frequency-space RG).

Results from the frequency+momentum-space RG are in excellent agreement with the 32^2 benchmark results. Equally important, however, is the enormous savings of storage and time which the momentum-space RG provides over comparable high-magnification calculations within the full Brillouin zone. (As noted above, high magnification is not crucial in this case, but is in the case which follows.) Timing and storage data from runs on a Cray Y-MP are summarized in Table I for the RG sequence described above and for a sequence of frequency-space RG calculations on meshes of various sizes. Note that an increase in the total number of Brillouin-zone points by a factor of 4 leads to an increase in computation time of roughly a factor of 16 if the integration region is the full Brillouin zone. In contrast, the CPU time per iteration in Table I for the frequency+momentum-space RG only increases from 2.5 to 3.0 sec in passing from the 32^2 to the 64^2 mesh using the momentum-space RG, and from 3.0 to 23 sec in passing from the 64^2 to the 128^2 mesh. (The factor of increase depends on the number of $\mathbf{k}$ points retained: If *all* points were retained after each rediscretization, the calculation time would increase by roughly a factor of 16. The actual number of points retained varies with the choice of Ω^K/t.) The total increase in time in passing from a 32^2 to a 512^2 mesh is only a factor of 440, considerably smaller than the expected increase for an FFT algorithm and a factor of 150 smaller than the increase for a brute-force algorithm.

In order to illustrate the sensitivity of the RG approach for detecting singularities, it is convenient to examine the form of the FLEX self-energy for a weak interaction strength at precisely half filling, where the Hubbard model's Fermi surface is perfectly nested. It has been demonstrated by Serene and Hess[6] that the imaginary part of the self-energy exhibits a delicate cusplike singularity in this case. As noted previously,[13] in the variant of the FLEX approximation considered here, we do not consider the exchange of singlet-pair fluctuations.[18] Nevertheless, the singularities which accompany the nested Fermi surface for arbitrarily weak U/t persist in our treatment. We follow Serene and Hess by plotting in Fig. 10,

$$\Sigma_2(\mathbf{k},i\pi T)/\pi T \equiv 1-Z_{\mathbf{k}}(T) , \tag{41}$$

along the Brillouin-zone diagonal $\Gamma-M$. The results shown here were obtained using the same combined frequency+momentum-space RG described above, this time with momentum-space cutoffs of $\Omega^K/t=1.51$, 0.75, and 0.38 for passing sequentially from a 64^2 mesh in the full Brillouin zone to a 512^2 mesh near the Fermi surface. Since the momentum-space RG automatically locates the Fermi surface, it is equally straightforward to treat singularities of this type at general fillings [e.g., for the parameter set used to generate Fig. 4(a)]. As stated previously, we defer a discussion of the physics at general fillings to a separate paper.[19]

The normal-state calculations presented here may be viewed as a preliminary to studies of the d-wave superconducting state which emerges in FLEX calculations away from half filling.[4] In order to locate the transition temperature T_c for the d-wave phase transition accurately, it is necessary to solve the linear eigenvalue problem

$$\int_{k'} V_{\text{sing}}(k-k';T)|G(k';T)|^2\phi(k';T)=\lambda_d(T)\phi(k;T) ,$$
$$\lambda_d(T)=1 \rightarrow T=T_c , \tag{42}$$

TABLE I. Memory and timing comparisons for the sample RG procedure used to produce Fig. 9. All calculations were performed on a Cray Y-MP. To benchmark the increase in performance brought about by the momentum-space RG, results are shown first for a pure factor-of-2 frequency-space RG operating within the full Brillouin zone on meshes of varying sizes (rows labeled "ω RG"). The second set of results was obtained using the sequential frequency+momentum-space RG described in the text (rows labeled "$\omega+\mathbf{k}$ RG"). Note that no timing results are shown for the pure frequency-space RG on the 256^2 and 512^2 meshes. Such calculations are impractical on the Cray Y-MP, i.e., the use of the momentum-space RG becomes essential at this point.

Mesh	32^2	64^2	64^2	128^2	128^2	256^2	512^2
T/t	0.03	0.03	0.015	0.015	0.0075	0.0075	0.0075
Memory (Mbytes)							
ω RG only	0.1	0.4	0.4	1.3	1.3	6.3	24
$\omega+\mathbf{k}$ RG	0.1	0.3	0.3	1.0	1.0	3.6	16
Time per iteration (CPU sec)							
ω RG only	2.5	38	38	344	344		
$\omega+\mathbf{k}$ RG	2.5	3.0	3.0	23	23	97	1 100
Time to convergence (CPU sec)							
ω RG only	5.5	410	611	4920	4576		
$\omega+\mathbf{k}$ RG	5.5	38	35	228	205	880	10 000

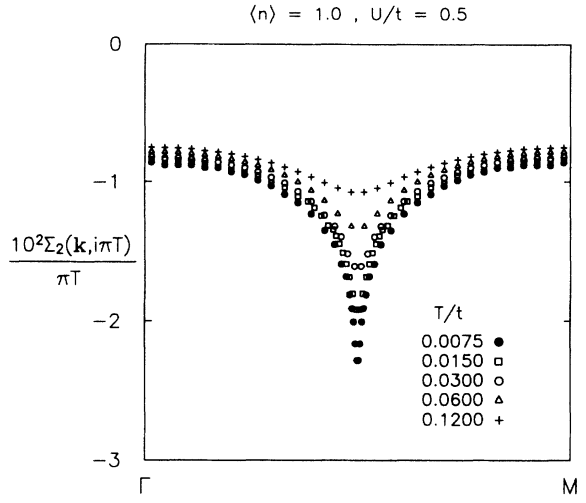

FIG. 10. Singular FLEX self-energy for the half-filled Hubbard model. The quantity $1-Z_{\mathbf{k}}(T)$ defined in the text is plotted along the Brillouin-zone diagonal for five different temperatures. As in Fig. 9, the results were obtained using a combined frequency+momentum-space RG. The effective mesh sizes are 64^2 ($T/t=0.12$ and 0.06), 128^2 ($T/t=0.03$), 256^2 ($T/t=0.015$), and 512^2 ($T/t=0.0075$).

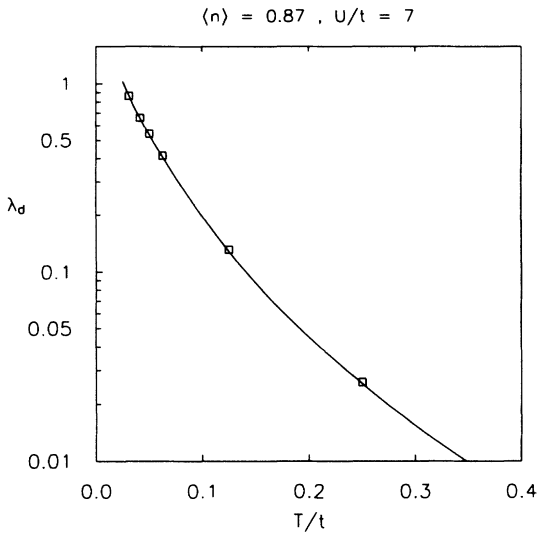

FIG. 11. Calculation of $\lambda_d(T)$, the d-wave instability eigenvalue. Results are shown for two calculations on a fixed 16^2 mesh. The model parameters are $U/t=7$ and $\langle n\rangle=0.87$. The squares were obtained by a brute-force technique, while the solid line is the result of a frequency-space RG with both factor-of-2 and fixed cutoff operations. The predicted transition temperature is $T_c/t=0.026$.

with

$$V_{\text{sing}}(q)=\tfrac{3}{2}U^2\frac{\chi(q)}{1-U\chi(q)}-\tfrac{1}{2}U^2\frac{\chi(q)}{1+U\chi(q)} . \tag{43}$$

In principle, a quantitative RG procedure may be applied to reduce this eigenvalue problem to an equivalent problem in a smaller variable domain; this is exactly the idea behind the so-called Coulomb pseudopotential[20] in electron-phonon models with frequency cutoffs of the order of the phonon Debye frequency. At this point, however, we prefer to solve the eigenvalue problem within the *full* frequency and momentum space, drawing the values of V_{sing} and $|G|^2$ from different RG variable domains, as in the calculation of $n_k(T)$ described above.

For simplicity, we restrict attention to frequency-space RG's with a fixed Brillouin-zone mesh. The frequency sum implicit in Eq. (42) for temperature $T=T_M$ may then be rewritten as

$$T_M\sum_{\omega_n(T_M)}\rightarrow\sum_{j=0}^{M}T_j\sum_{\Omega_{j+1}<|\omega_n(T_j)|<\Omega_j} , \tag{44}$$

where, as before, $\Omega_{M+1}\equiv 0$. The required values of $|G|^2$ have been previously stored, and the values of χ required for computing V_{sing} have either been stored or may be calculated accurately by interpolation. Results are shown in Fig. 11 from two calculations of the instability eigenvalue $\lambda_d(T)$ for the parameter set $U/t=7$ and $\langle n\rangle=0.87$ with an initial frequency cutoff $\Omega_0/t=25$ and a 16^2 Brillouin-zone discretization. The first calculation (squares) begins at $T_0/t=1$ and proceeds down to $T/t=0.031\,25$ with no frequency-space RG. The number of positive fermion frequencies increases from $N(T_0)=4$ to $N(T)=128$. The second calculation (solid line) again begins at $T_0/t=1$ and then employs the factor-of-2 frequency-space RG to reach $T_4/t=0.0625$. From this point, the transition temperature is approached smoothly by maintaining a constant cutoff and slowly increasing $N(T_i)$ (see Sec. III A). In this case the eigenvalue reaches unity near $T_{15}/t=0.025$, where $N(T_{15})=28$. The results of the two calculations are in excellent agreement, but the second approach is more than 40 times faster than the first. (This advantage may be improved even further by continuing the factor-of-2 RG procedure to lower temperatures.)

V. CONCLUSIONS

The FLEX approximation, a Baym-Kadanoff generalization of Hartree-Fock theory, has been used in the present work to investigate frequency-space and momentum-space renormalization groups for the simplest 2D Hubbard model. Frequency-space renormalization groups have been previously applied in the solution of a more complex approximation, the so-called "basic parquet," for the effectively zero-dimensional Anderson impurity model.[14] In both studies RG methods have produced gains in computation time and storage which allow the treatment of previously unreachable parameter regimes. As noted previously, the factor-of-2 frequency-space algorithm used in the present work requires computation time which scales roughly as $|\ln T|$ at low temperatures, in comparison with brute-force and FFT algorithms which scale as T^{-2} and $T^{-1}|\ln T|$, respectively.

Due to the simplicity of the basic on-site interaction in the Hubbard model, the FLEX approximation for one-electron Green's functions may be renormalized using only two functions, $\Delta\Sigma(k)$ and $\Delta\chi(q)$. In order to inves-

tigate two-particle correlation functions, it is necessary to renormalize more complicated vertex functions as well. Such a vertex renormalization has already been successfully carried out within the basic parquet for the Anderson impurity model.[14] It is conceptually much simpler to carry out a vertex renormalization within the FLEX approximation, since two-particle vertices may be expressed directly in terms of self-consistent one-particle self-energies;[11-12] in contrast, the basic parquet requires that the two-particle vertices themselves satisfy a complicated set of consistency relations (the parquet equations).[11,14] The only complication in setting up vertex renormalization for the 2D Hubbard model within FLEX arises from storage limitations. Since the vertex functions depend on three independent "three-momenta" k, they cannot be stored in full generality on the same meshes used in the one-particle studies reported above. The problem of intelligently calculating two-particle correlation functions is a major area for further investigation.

A second area which requires further study is the use of RG techniques in broken symmetry phases. As remarked earlier, the Coulomb pseudopotential[20] introduced in the early 1960s is a semiquantitative RG construct for treating electron-phonon superconductivity using a frequency cutoff of the order of the Debye energy, rather than the electronic bandwidth. A quantitative RG treatment of superconductivity in simple model approximations requires a renormalization of the off-diagonal self-energy ϕ, as well as the diagonal self-energy Σ treated above. Even within the FLEX approximation, this is a considerably more involved task than the treatment of the normal state.

ACKNOWLEDGMENTS

This work was supported in part by the National Science Foundation under Grant No. DMR92-12971, and by the Alfred P. Sloan Foundation (N.E.B.). Supercomputer calculations were performed on the Cray Y-MP at the San Diego Supercomputer Center.

---

[1]For a broad survey of recent theoretical work in this area, see, e.g., *Strongly Correlated Electron Systems III,* edited by G. Baskaran *et al.* (World Scientific, Singapore, 1992).

[2]For a compendium of theoretical articles on the Hubbard model from the years 1963 to 1990, see *The Hubbard Model: A Reprint Volume,* edited by A. Montorsi (World Scientific, Singapore, 1992).

[3]N. E. Bickers and D. J. Scalapino, Ann. Phys. (N.Y.) **193**, 206 (1989).

[4]N. E. Bickers, D. J. Scalapino, and S. R. White, Phys. Rev. Lett. **62**, 961 (1989).

[5]N. E. Bickers and S. R. White, Phys. Rev. B **43**, 8044 (1991).

[6]J. W. Serene and D. W. Hess, Phys. Rev. B **44**, 3391 (1991).

[7]J. Luo and N. E. Bickers, Phys. Rev. B **47**, 12 153 (1993).

[8]C.-X. Chen and N. E. Bickers, Solid State Commun. **82**, 311 (1992).

[9]A. B. Migdal, Zh. Eksp. Teor. Fiz. **34**, 1438 (1958) [Sov. Phys. JETP 7, 996 (1958)].

[10]G. M. Eliashberg, Zh. Eksp. Teor. Fiz. **38**, 966 (1960) [Sov. Phys. **JETP 11**, 696 (1960)].

[11]For pedagogical reviews of these extensions, see e.g., N. E. Bickers, in *Quantum and Classical Many-Body Theory in Condensed Matter Physics,* edited by G. Giuliani and G. Vignale (World Scientific, Singapore, 1993); N. E. Bickers, in *Strongly Correlated Electron Systems II,* edited by G. Baskaran *et al.* (World Scientific, Singapore, 1991), p. 253.

[12]G. Baym and L. P. Kadanoff, Phys. Rev. **124**, 287 (1961); G. Baym, *ibid.* **127**, 1391 (1962).

[13]The effective potential V_{eff} used here represents the exchange of spin and charge fluctuations. We choose to neglect the exchange of singlet-pair fluctuations, which are included in the treatments of Refs. 4–7. This exclusion has only a minor effect on calculated quantities at general fillings, but greatly simplifies the FLEX treatment of possible superconducting states, which we intend to investigate in future work. The RG treatment of the normal-state equations with singlet pairs included would be equally straightforward.

[14]N. E. Bickers and C.-X. Chen (unpublished).

[15]In analogy with the conventional solution technique for the Eliashberg equations (Ref. 10), we converge the FLEX equations using 0.01% convergence criteria for $\mathrm{Re}\Sigma(k)$, $\mathrm{Im}\Sigma(k)/\omega_n$, and $\chi(q)$. The use of the quantity $\mathrm{Im}\Sigma/\omega_n$ [often denoted $1-Z(k)$ in Eliashberg theory], rather than simply $\mathrm{Im}\Sigma(k)$, places additional emphasis on the region of low frequencies. Note that our self-energy plots also display $\mathrm{Re}\Sigma(k)$ and $\mathrm{Im}\Sigma(k)/\omega_n$.

[16]Real-frequency functions can be calculated from imaginary-frequency data by performing a numerical analytic continuation. To accommodate errors of the order of 1% in imaginary-frequency data, the most appropriate continuation technique may be maximum likelihood estimation (the so-called "maximum entropy" approach).

[17]When the effective potential is strongly temperature dependent (e.g., in the vicinity of an antiferromagnetic phase transition), the estimate in Eq. (32) may break down. It is then important to monitor the stage-by-stage success of the momentum-space RG directly.

[18]The present approximation is inappropriate for a detailed study of half filling since it breaks the symmetry between charge and singlet-pair excitations at this point.

[19]C.-H. Pao and N. E. Bickers (unpublished).

[20]P. Morel and P. W. Anderson, Phys. Rev. **125**, 1263 (1962).

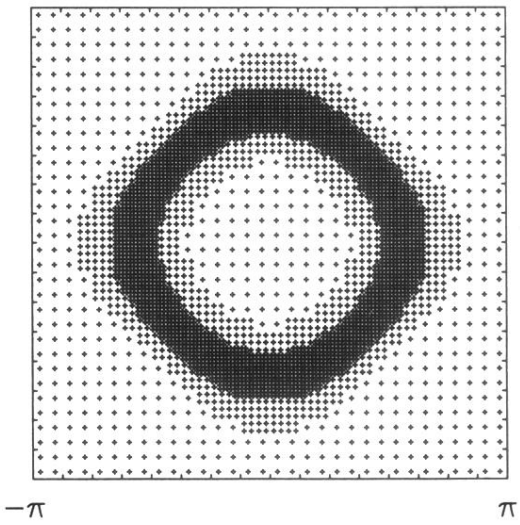

FIG. 3. Brillouin-zone discretization for a sample momentum-space renormalization group. Three stages are illustrated. The initial mesh has 32^2 points, while the next two meshes have reduced areas, with scales corresponding to 64^2 and 128^2 points within the full zone. The cuts were made for the FLEX approximation with $U/t=8$ and $\mu/t=-3$, corresponding to filling $\langle n \rangle=0.53$ at zero temperature. The energy cutoffs are $\Omega_1^K/t=1.51$ and $\Omega_2^K/t=0.76$.